RESEARCH ARTICLE

A Novel, Simple, and Flexible Fault-Tolerant Control Algorithm for Multiphase Electrical Machine Operation Under Open Circuit Faults

**MASSIMO CARUSO [ID], ANTONINO OSCAR DI TOMMASO,
AND ROSARIO MICELI [ID], (Member, IEEE)**
Department of Engineering, University of Palermo, 90128 Palermo, Italy
Fondazione MOST—Centro Nazionale per la Mobilità Sostenibile, 20158 Milan, Italy

Corresponding author: Massimo Caruso (massimo.caruso16@unipa.it)

ABSTRACT This paper presents a novel and simple procedure for the determination of a Fault-Tolerant Algorithm (namely FTA) for the adequate working operation of an electric machine equipped with a general m-phase winding under possible open circuits occurring in some of its phases. The FTA is firstly theoretically derived from the analysis of the magnetic field distribution in polyphase systems, then simulated through finite-element analysis and finally implemented via software for real-time validation. The effectiveness of the proposed procedure is confirmed through experimental tests on a laboratory setup. Key contributions include the flexibility of the algorithm, which can be applied to any m-phase electric machine with various winding configurations. Both the obtained FEA and experimental results demonstrate that the proposed control algorithm can be easily used and applied in electric drives supplied by m-phase motors under fault conditions without significantly affecting the magnetic performance of the whole system and ensuring the continuity of operation even in the presence of faults.

INDEX TERMS Multiphase machines, fault-tolerant operation, finite element analysis, IPMSM, induction motors.

I. INTRODUCTION

Over the past decades, multiphase machines have gained significant relevance in both the scientific and industrial communities, due to their intrinsic features of fault-tolerant capability, which brings undoubted advantages to many

The associate editor coordinating the review of this manuscript and approving it for publication was Wei Xu [ID].

applications in which safety is a very critical aspect, such as aerospace and automotive, providing also higher efficiency and flexibility concerning their three-phase counterparts [1], [2]. However, it appears evident that the adoption of a higher number of phases leads to a higher complexity during the design phase of the machine, as well as for the control methods to be adopted for the related electric drive [3], [4]. Therefore, an optimal compromise between safety and

complexity is one important issue faced worldwide by many researchers in the recent literature, leading to the need of providing accurate algorithms capable of detecting fault conditions, allowing the machine to operate even in critical conditions during short-circuits or open-circuit of some of the phases supplied by the electrical drive.

In this scenario, since when the first prototypes of multiphase machines were realized in the late '60s [5], several control strategies have been developed to detect and face fault conditions occurring in one or more phases of the machine, allowing the continuity of operation of the related drive system [6], [7], [8], [9], [10], [11], [12]. More in detail, two main categories of control strategies can be identified, covering the possible faults of different nature, such as Open Circuit Faults (OCF), Short Circuit Faults (CSF) between the interturns of the winding or at its terminals, and so on. The first category is represented by the *passive methods*, which do not consider any information about the specific fault, but take into account the worst-case scenario in the early design stage of the system and integrate robust control, providing stability in the system. Some of these methods are presented in [13], [14], [15], [16], [17], and [18], highlighting the drawback that, in case of several unpredictable faults, the stability of the system can be seriously compromised. On the other hand, the second category is represented by active methods, which are based on acquiring a detailed knowledge of the actual fault occurring in the system and acting consequently to ensure stable operation even in critical conditions. The accuracy of this information is, clearly, crucial for the proper effectiveness of the control strategy, which is typically based on either changing the parameters of the controller (fault accommodation strategy) or modifying its structure (reconfiguration strategy).

In any case, many strategies have been presented in the recent literature to achieve optimal post-fault steady-state performances. Some of them are focused on the theories of Artificial Neural Networks (ANNs) [19] and Fuzzy Logic (FZ) [20], [21], [22], where the development of a Knowledge Base allows the implementation of the rules in the Expert System, which also provides the data processing for the fault diagnosis. Other recent studies have proposed techniques based on the energy entropy change in the whole drive system [23], where the diagnosis is achieved by computing the empirical mode decomposition energy entropy of the currents flowing through the *m*-phase machine, or on the theory of symmetrical components, in which the fault-tolerant condition can be identified by analyzing the system degradation in terms of possible unbalanced conditions of the electrical quantities involved in the machine after the OCF or SCF [24], [25]. Further methods consider the adoption of different winding layout arrangements [26], or the dynamic model of the machine that adopts either state or parameter estimation [27], [28].

The fault-tolerant operation of multiphase machines can be optimally achieved by imposing the same copper losses for both pre-fault and post-fault operations [29], [30], or by limiting the magnitude of the currents during the fault condition

at their pre-fault values [31]. Either way, the methodology consists of maintaining a conservative criterion of the crucial quantities involved in the system. However, it has been demonstrated that the second methodology could generate significant torque ripple, determining high vibrations and, consequentially, the potential breakdown of the system [32].

In this context, this paper presents a simple and generalized procedure for the adequate working operation of a multiphase machine under possible open circuits occurring in some of its phases, which represents the most common fault condition during the operation of electric machine drives. This procedure, which leads to the development of a Fault Tolerant Algorithm (FTA), can be applied to both synchronous and induction machines equipped with any configuration of *m*-phase winding, from the normal to the non-redundant reduced type [33] and it is based on the theory of the magnetic field distribution in polyphase systems, from which a general formula for the spatial distribution of phase current phasors can be derived to provide a conservative magnetic field even in the case of open-circuits. After describing the theoretical aspects that regulate the operation of the proposed algorithm through the generalized concept regarding non-redundant polyphase systems, the work is focused on demonstrating through FEM simulations that the magnetic behavior of the electric machine during a possible fault condition is not been significantly varied thanks to the adoption of the proposed FTA. Besides the magnetic performance of the motor, the validity of the algorithm is also applied experimentally to an electrical drive to analyze its dynamic performance in terms of reconfiguration time and quality of waveforms, demonstrating the effectiveness of the proposed theory.

The theoretical procedure that allows the development of the FTA is firstly described in Sections II and III, then simulated through finite-element analysis in Section IV and finally experimentally validated by employing a laboratory setup reported in Section V.

II. MAGNETIC FIELD PRODUCED BY AN M-PHASE WINDING

For an *m*-phase electrical machine with N slots, p pole pairs and q slots per pole per phase (*e.g.*, $N/2m$ coils for each phase section), the general formula of the spatial distribution of the magnetic flux density field generated by the *k-th* phase section at the working harmonic $\nu = 1$ is given by:

$$b_{1k}(x,t)$$
$$= \frac{\mu_0 w k_{w1}}{\pi p \delta} cos\left[\frac{\pi}{\tau}(x - x_0 - x_{0k})\right] \cdot$$
$$\cdot I_{xk} cos\left[\omega t - \emptyset_k\right] = B_{1xk} cos\left[\frac{\pi}{\tau}(x - x_0 - (k-1)\frac{\tau}{m})\right] \cdot$$
$$\cdot cos\left[\omega t - \emptyset_k\right] \quad (1)$$

where μ_0 is the permeability of air, $w = pqs$ (s is the number of turns), k_{w1} is the winding factor of the working harmonic, x_{ok} is the phase-shift between the magnetic axes, τ is the pole pitch, B_{xk} is the maximum value of the spatial distribution of the magnetic flux density field and I_{xk} is the amplitude of the

current flowing through the phase k with proper phase-shift ϕ, which is supposed to possess the following variability:

$$i_k(t) = I_{xk} \cdot \cos[\omega t - \emptyset_k] \tag{2}$$

In addition, it is well known that a pulsating wave can be represented by the composition of two waves, namely v_1^+ and v_1^-, with equal amplitude (half of the amplitude of the initial wave), propagating in opposite directions, as shown in Fig. 1. This decomposition can also be analytically discussed by expressing (1) as the sum of two spatial cosine waves: the first one, b_{1k}^+, rotates clockwise and is known as a progressive wave, while the second one, b_{1k}^-, rotates counterclockwise and is defined as a regressive wave.

$$
\begin{aligned}
b_{1k}(x,t) \\
&= b_{1k}^+(x,t) + b_{1k}^-(x,t) = \\
&= \frac{B_{1xk}}{2} \left\{ \cos\left[\frac{\pi}{\tau}\left(x - x_0 - (k-1)\frac{\tau}{m}\right) - \omega t + \emptyset_k \right] \right. \\
&\left. + \cos\left[\frac{\pi}{\tau}\left(x - x_0 - (k-1)\frac{\tau}{m}\right) + \omega t - \emptyset_k \right] \right\}
\end{aligned}
\tag{3}
$$

By considering (3) and the overall effect due to the m phases of the corresponding winding, the distribution of the air-gap flux density field is given by:

$$
\begin{aligned}
b(x,t) \\
&= \sum_{k=1}^{m} \left[b_k^+(x,t) + b_k^-(x,t) \right] = \\
&= \frac{B_x}{2} \sum_{k=1}^{m} \left\{ \cos\left[\frac{\pi}{\tau}\left(x - x_0 - (k-1)\frac{\tau}{m}\right) - \omega t + \emptyset_k \right] \right. \\
&\left. + \cos\left[\frac{\pi}{\tau}\left(x - x_0 - (k-1)\frac{\tau}{m}\right) + \omega t - \emptyset_k \right] \right\}
\end{aligned}
\tag{4}
$$

The *rms* values of all the m-phase currents are considered with equal magnitude, which implies that $B_{x1} = B_{x2} = \ldots = B_{xm} = B_x$.

For a proper working operation of the system taken into account, it appears evident that the rotating (linear) magnetic field must be produced with the same constant amplitude, even in the case of a fault that involves one or more phases of the electric machine. Therefore, the working phases must be driven by an unbalanced system of currents in which the phase shifts Φ_k are given by the following equation:

$$\Phi_{k_{1,\ldots,m}} = (k-1)\frac{m+1}{m-1}\gamma \tag{5}$$

where

$$
\gamma = \begin{cases}
\dfrac{\pi}{m} & \text{for reduced systems} \\[2mm]
\dfrac{2\pi}{m} & \text{for non-reduced systems}
\end{cases}
\tag{6}
$$

In this case, the amplitude of the corresponding flux density field is decreased by a factor k_g equal to:

$$k_g = \frac{\sin\gamma}{\sin\left(\frac{\gamma}{m-1}\right)} \tag{7}$$
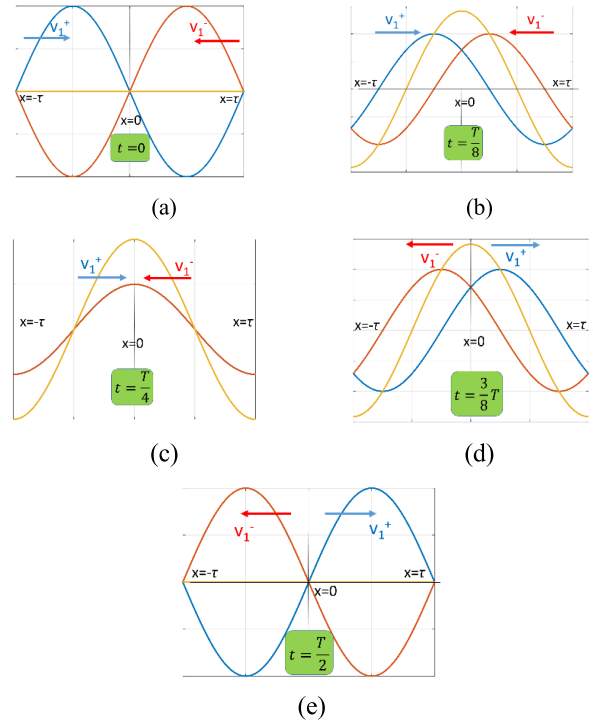
FIGURE 1. Representation of the composition of a pulsating wave during different time instants: (a) t = 0, (b) t = T/8, (c) t = T/4, (d) t = 3/8T, (e) t = T/2.

Eq. (5) can be deduced from (4) by imposing that the regressive wave b_{1k}^- must be canceled:

$$-(k-1)\gamma - \Phi_{gk} = -(k-1)\frac{2\pi}{m-1} = -(k-1)\frac{2m}{m-1}\gamma \tag{8}$$

Therefore, to maintain the invariance of the amplitude of the magnetic field during a fault, the amplitudes of the currents must be increased by k_{gi}, namely amplitude factor, equal to:

$$k_{gi} = m\frac{\sin\left(\frac{\gamma}{m-1}\right)}{\sin\gamma} \tag{9}$$

The equations (7) and (9) highlight the fact that the increasing factors of both flux density and current are strictly related to the number of healthy phases that operate in the system with the aim of maintaining the same generated rotating magnetic field.

In the general case of g faults in the phases of an electrical machine, the angle shifts must be modified as follows:

$$\Phi'_{gk} = (k-1)\frac{m+g}{m-g}\gamma \tag{10}$$

where g is the number of fault phases.

By imposing the same condition of (8), the flux density field must be equal to:

$$b'^{(x,t)} = \sum_{k=1}^{m-g} \left[b_k^+(x,t) + b_k^-(x,t) \right] =$$

$$= \frac{B_x}{2} \sum_{k=1}^{m-g} \left\{ \cos\left[\frac{\pi}{\tau}(x - x_0) - (k-1)\gamma\right] \right.$$

$$\left. \cdot \cos\left[\omega t - (k-1)\frac{m+g}{m-g}\gamma\right]\right\}$$

$$= \frac{B_x}{2} \sum_{k=1}^{m-g} \left\{ \cos\left[\frac{\pi}{\tau}(x - x_0) - \omega t + \varphi_k^+)\right] \right.$$

$$\left. + \cos\left[\frac{\pi}{\tau}(x - x_0) - \omega t + \varphi_k^-)\right]\right\} \qquad (11)$$

For instance, the representation of the wave propagation evolution for a seven-phase system of currents in the cases of no-faults, open-circuit on phase no. 7, two open-circuits on phase no. 6-7 and three open circuits on phases no. 5, 6 and 7 are reported in Fig. 2 (a)-(d), respectively. It can be noted that the normalized amplitudes of the currents are increased by the factor k_{gi} computed from (9) and the mutual phase shift is modified according to (10) depending on the number of faults occurring in the system.

Finally, the corresponding phase shifts in the phasor diagram can be easily determined by considering the following equations:

$$\theta_{base} = \gamma \cdot \left(\frac{m+g}{m-g}\right) \qquad (12)$$

$$\theta_i = (i-1) \cdot \theta_{base} \qquad (13)$$

As shown in the next Sections, this general procedure can be applied in both *reduced* and *normal* polyphase systems [33]. The first category is characterized by a spatial distribution of their m phases within the $[0, \pi[$ interval. In this case, the presence of a homopolar component leads to the adoption of a neutral conductor, unless the odd group of phasors are spatially overturned. In the case of an odd number of phases ($m \in O$), the system can be always converted to a pure system by changing the polarities of the currents circulating in the even phases. In this case, the system can be defined as *normal*.

III. DESCRIPTION OF THE FAULT-TOLERANT CONTROL ALGORITHM

The mathematical formulation described in Section II has been implemented via software through a control algorithm, namely FTA (Fault-Tolerant Algorithm), whose flow diagram is shown in Fig. 3.

The process starts with the definition of the number of phases, the type of system (*reduced* or *normal*) and the number of faults that eventually occurred in the system (if the system runs with no faults, g is set equal to zero). The clear identification of the non-redundant system is crucial to setting the equation that specifically regulates the polyphase configuration, as γ assumes different values in the two cases.

Based on these defined input parameters, the FTA computes the spatial distribution of the magnetic flux density field from the composition of the two progressive and regressive waves, by following equations (4) – (10). In such a way, the sinusoidal trends in time of the m-phase current system can be
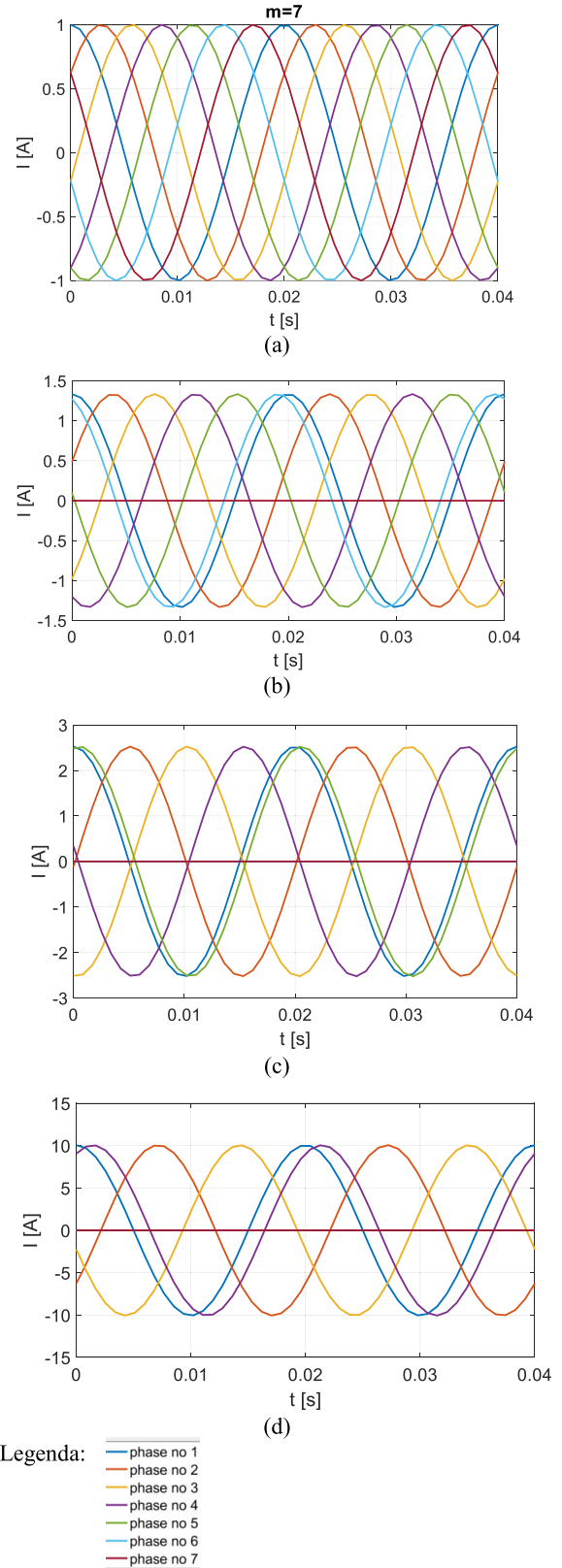
FIGURE 2. Wave propagation evolution for a seven-phase system with (a) no faults, (b) fault on phase no. 7, (c) faults on phases no. 6 and 7, (d) faults on phases no. 5, 6 and 7.

determined and plotted to verify the corresponding adequate amplitudes (eventually increased by the factor k_{gi}), the phase
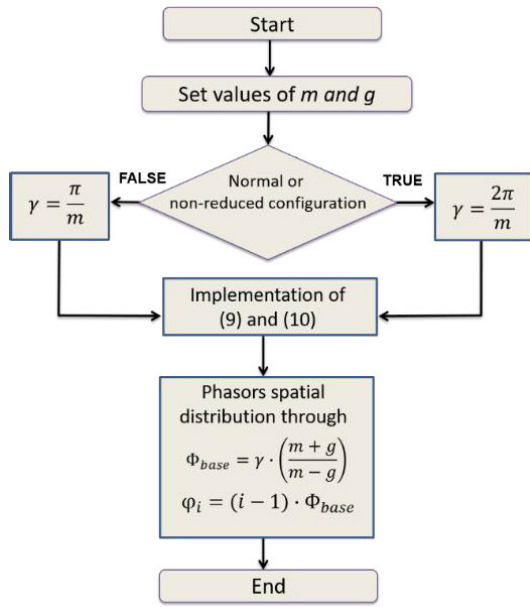
FIGURE 3. Flow diagram of the control algorithm.

(a) $g=0$, $\varphi_{base}=72°$ (b) $g=1$, $\varphi_{base}=108°$

(c) $g=2$, $\varphi_{base}=168°$ (d) $g=3$, $\varphi_{base}=288°$

FIGURE 4. Spatial distribution of the phasors for a normal five-phase winding configuration in the cases of: (a) no faults, (b) one fault, (c), two faults and (d) three faults.

shifts between the propagating waves and the number of possible faulted phases.

Afterward, the spatial phase shifts between the phasors of the polyphase system and is computed based on (11) - (13), so that the spatial distribution of the phasors can be computed, which allows the determination of the final configuration that drives the electric machine. As a result, from the knowledge of input g, the FTA provides the spatial configuration of the m-g phase currents, defining the values of k_{gi} and θ_i. In the meanwhile, as a term of comparison, it also plots the m phasors with their specific phase shifts in a no-fault operating condition. Finally, from this spatial distribution, the algorithm defines the corresponding input reference currents (in amplitude and phase shift) to be used in the related control system.

In the event of an additional fault, the algorithm resets the configuration by dynamically recalculating the phase shifts of the phasors and their renewed equal amplitudes, based on equations (4)-(13), re-plotting the waveforms and re-distributing the spatial phasors. This self-adjusting capability ensures the continued adaptability and fault tolerance of the system, enhancing its flexibility in the face of evolving operational challenges.

For example, Fig. 4 shows the phasors disposition of the currents in the possible cases of (a) no faults, (b) fault in phase no. 5, (c) two faults and (d) three faults for a five-phase electrical machine equipped with a normal winding configuration.

It has to be remarked that the new asymmetric disposition of the stator current phasors leads to the presence of a zero-sequence current component that has necessarily to flow in the neutral conductor to ensure a return path.
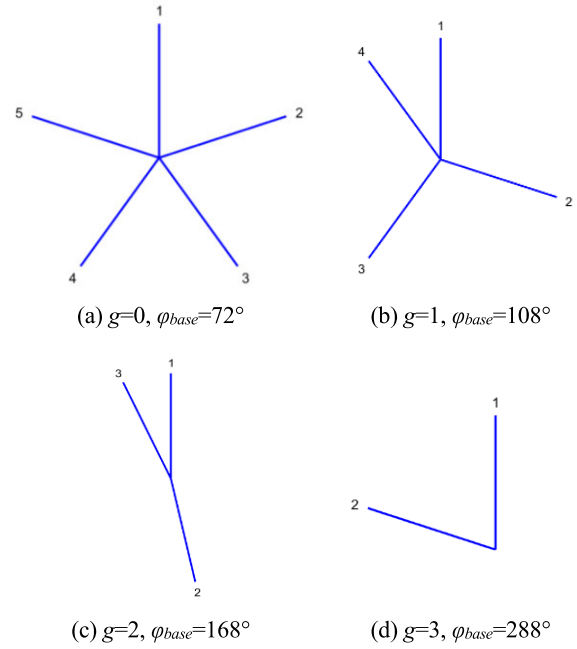
Therefore, for this type of fault-tolerant technique, the presence of the neutral conductor connecting the center of the phasor star to the DC link midpoint, especially in the two-phase operating condition (*i.e.*, Fig. 4 (d) and Fig. 5 (e)).

As mentioned in the previous Section, the described procedure can be also applied to non-redundant reduced configurations, such as the commonly adopted dual-three-phase scheme, as reported in Fig. 5. As well as for the previous case, the algorithm can adequately shift the phasors of the currents in case of single or multiple faults, as shown in Fig. 5 (b)-(d) for faults from one to four faults, respectively. It has to be highlighted that the odd group of phasors (phases no. 3 and 4 for this particular case) has to be spatially overturned after the determination of the corresponding phase shifts. In such a way, by considering the theoretical explanation of Section II, the rotating magnetic field can be still generated, allowing the operation of the electric drive even with many faults occurring in multiple phases of the electrical machine. Therefore, the working healthy phases must be driven by an unbalanced system of currents in which the amplitude and the phase shifts are given by (9) and (13). Table 1 summarizes the values of k_{gi} related to all the configurations of both Figs. 4 and 5, as well as the related phase shifts.

IV. SIMULATION RESULTS

The Finite Element Analysis has been considered to demonstrate the effectiveness of the proposed procedure. More in detail, the model of a five-phase IPMSM (Interior Permanent Magnet Synchronous Machine) with 30 slots and 3 pole pairs has been considered as a reference structure, as shown in Fig. 6 (a).

(a) g=0, φ_{base}=30° (b) g=1, φ_{base}= 42°

(c) g=2, φ_{base}= 60° (d) g=3, φ_{base}= 90°

(e) g=4, φ_{base}= 150°
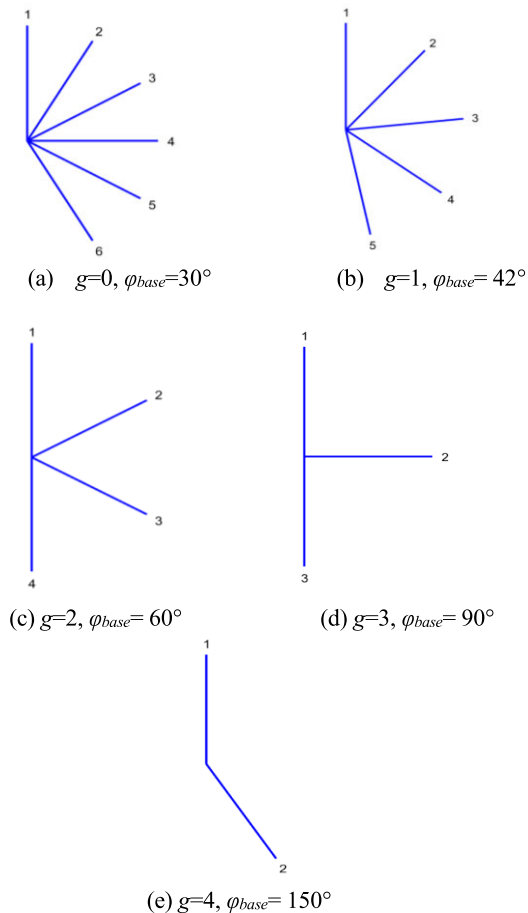
FIGURE 5. Spatial distribution of the phasors for a reduced dual three-phase winding configuration in the cases of: (a) no faults, (b) one fault, (c), two faults and (d) three faults.

TABLE 1. Current amplitude increase for different fault conditions.

Phase number	Number of faults	Value of k_g	Phase shift sequence of healthy phases
m=5	g=1	1.32	0°, 108°, 216°, 324°
	g=2	2.13	0°, 168°, 336°
	g=3	3.09	0°, 288°
m=6	g=1	1.25	0°, 42°, 84°, 126°, 168°
	g=2	1.56	0°, 60°, 120°, 180°
	g=3	2.08	0°, 90°, 180°
	g=4	3.10	0°, 150°

This model is equipped with 12 NdFeB permanent magnets that magnetize the machine in both the radial and tangential directions. Further geometrical and electrical data are summarized in Table 2, whereas the corresponding plane scheme of the double-layer winding is depicted in Fig. 6 (b).

The performances of the previously described model are analyzed by using a FEM (Finite Element Method) approach by employing the FEMM4.2® software, which is based on three different steps. The first one, named *pre-processing*, is focused on the geometry definition and the assignment of the materials, the boundaries that characterize the structure

TABLE 2. Rated values and geometrical data of the IPMSM.

Quantity	Value
Voltage [V]	132
Current [A]	3.6
Speed [rpm]	4000
Torque [Nm]	1.8
Number of pole pairs	3
Stator resistance [Ω]	2.21
Magnetic permeability of stator core [H/m]	$6.3 \cdot 10^{-3}$
Magnetic permeability of laminations [H/m]	$2.5 \cdot 10^{-1}$
Magnetic flux density of PMs [MGOe]	40
Outer stator diameter [mm]	81
Inner stator diameter [mm]	49.6
Outer rotor diameter [mm]	48
Inner rotor diameter [mm]	18.46
Axial rotor length [mm]	59
PM thickness [mm]	3
Air-gap [mm]	0.8
PM type	NdFeB
PM width [mm]	13.45

(the *Dirichlet* boundary conditions were set with potential $A = 0$) and the currents on each of the five-phase winding. The second step (namely *solution*) is characterized by the determination of the FEM solution from the creation of the related mesh (for this simplified model, the automated mesh generated almost 120000 nodes). Finally, the third step, namely *post-processing*, allows the evaluation of the results obtained from the simulation from the processing of the solution. Therefore, the FEM analysis has provided the determination of the trends and values of the main electrical and magnetic quantities concerned with the machine model, such as the air-gap flux density field and both its radial and tangential components, the magnetic forces and the static characteristic.

The FEM approach has been applied to the same IPMSM model, but simulating different fault conditions and, therefore, integrating the proposed fault-tolerant algorithm into the simulation and following the flow diagram of Fig. 3. The determination of these trends has been obtained from several FEM simulations by varying the angular position δ of the rotor from 0° to 360° with steps of 0.5°, achieving more than 700 rotor positions and, consequently, more than 700 values of the analyzed quantities for each condition of operation (with faults or no-faults).

Three sets of simulations were performed to verify the proposed algorithm's effectiveness. More in detail, in the first set of simulations, the performances of the machine in terms of flux density field as a function of the linear coordinate x, which is measured along the mid-air-gap circumference, as well as the unbalanced magnetic forces and the generated torque as a function of the load angle that has been evaluated at no-fault conditions.

Then, in the second set, a fault was simulated on phase no. 5, leading to the need to re-setting the phasor distribution of the *m-1* currents according to the proposed procedure implemented by the algorithm described in Sections III and IV.

(a)

(b)
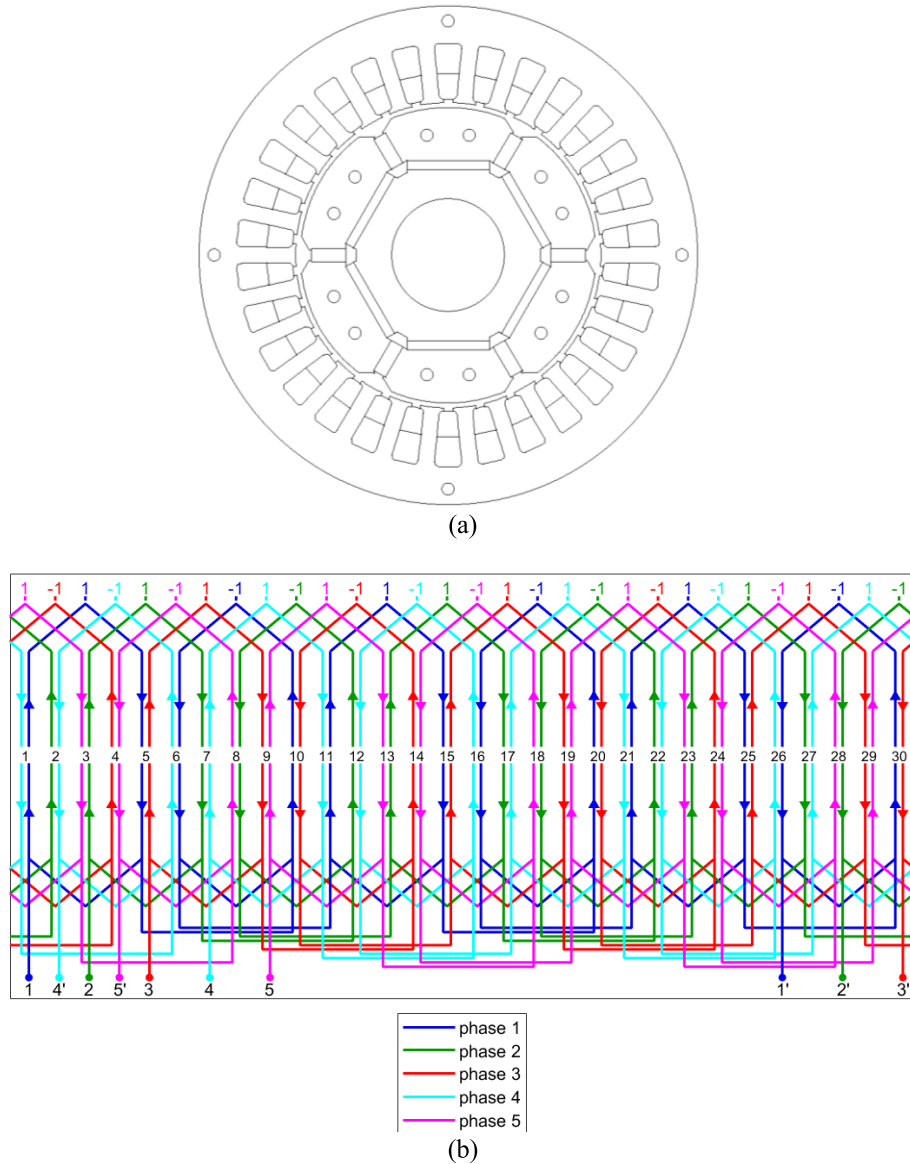
FIGURE 6. (a) Cross section of the reference IPMSM structure and (b) winding plane scheme.

Finally, two faults have been implemented in the model in the third set of simulations and the same electrical and magnetic quantities have been examined to provide another term of comparison.

A first comparison between the results obtained from sets A, B and C is shown in Fig. 7, which depicts the trends of the air-gap flux density field values as a function of x at $\delta = 0°$ for the three operating conditions (no fault: blue color, one fault: red color, two faults: green color). It appears clear that the proposed algorithm has allowed the maintenance of almost the same amplitude and trend of the flux density field concerning the no-fault condition.

The corresponding flux density plots are reported in Fig. 8 (a-c). For each condition, it can be noted that both the flux distribution and the density plot confirm that the areas affected by a higher magnetic field are confined within the stator teeth and yoke, ranging up to 1.2 T, whereas the
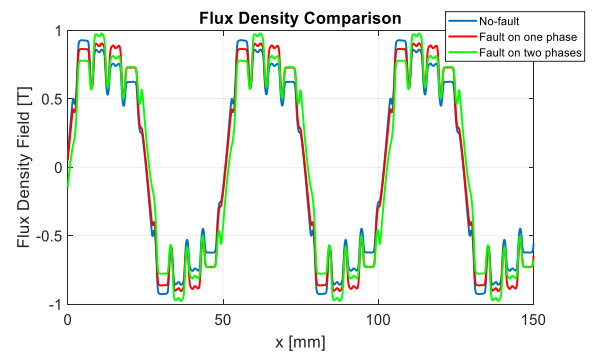
FIGURE 7. Flux density field comparison.

values of the air-gap flux density field are slightly below 1 T. Moreover, the same figure shows the current density plots for the three models, which highlights the presence of one or multiple faults in the IPMSM structure.
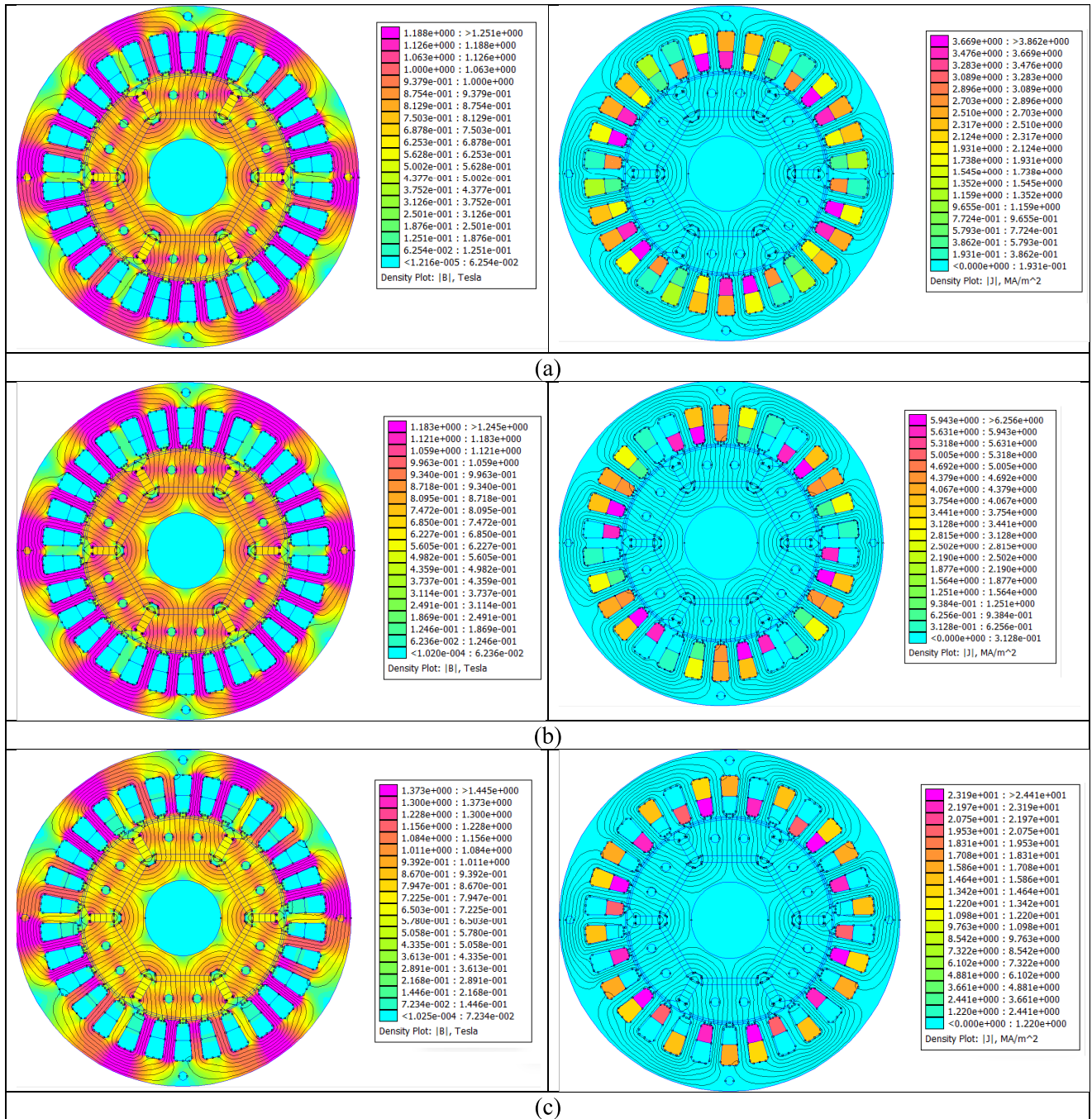
FIGURE 8. Flux density field and current density plots of the IPMSM structure for (a) *g = 0*, (b) *g = 1* and (c) *g = 2*.

Further results can be evaluated in Fig. 9, which shows the comparison between the generated torque as a function of the angular position of the rotor for the three operating conditions of no-fault (blue line), one fault (red line) and two faults (green line). As well as for the previous graphic, it can be noted that the algorithm has provided the condition of maintaining almost the same trend of produced torque, with a higher maximum value due to the increase of the currents by the factor k_{gi}. However, the machine's operation in fault conditions should be limited in time to avoid the risk of overheating due to the overcurrent application in the healthy phases, which could affect the integrity of the drive.

The proposed algorithm does not significantly affect the magnitude of the air-gap Maxwell stress tensor acting on the structure: as shown in Fig. 10, it is evident that the comparison provides almost similar trends of the previously mentioned forces. The Maxwell stress tensor in a generic point p of
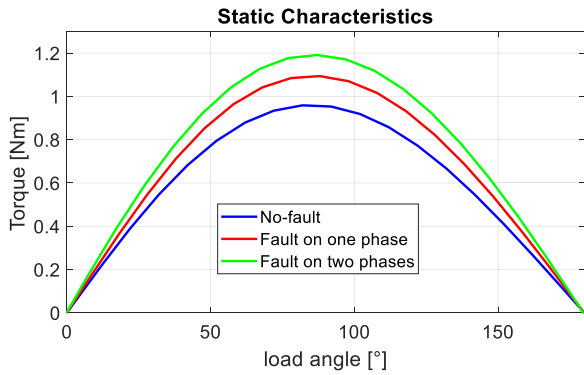
FIGURE 9. Comparison between the static characteristics.
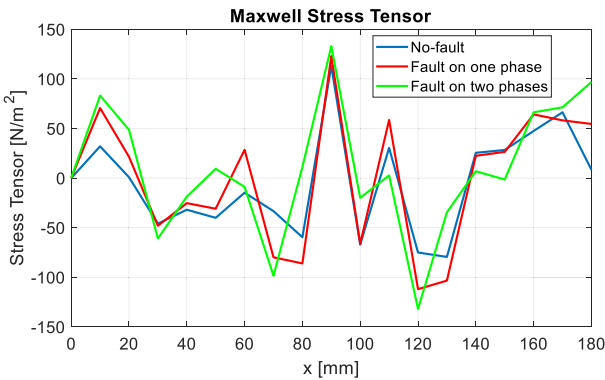
FIGURE 10. Comparison between the Maxwell stress tensor.

interest has been computed through the following equation:

$$\sigma_p = \frac{1}{2}(H(B \cdot n) + B(H \cdot n) - (H \cdot B)n) \qquad (14)$$

where H and B are the magnetic field and flux density field values detected in p, respectively, and n denotes the normal direction to the surface at the point of interest.

In addition, the current profiles for the specific cases of $g = 1$, $g = 2$ and $g = 3$ for this specific case of study are plotted in Fig. 11 (a-c).

Finally, Table 3 compares further results obtained from the FEM analysis of the three different models. In particular, it can be noted that both the average flux density through a pole and the magnetic field energy stored in the air gap are comparable even with the presence of open circuit conditions. On the other hand, the double fault operation leads to higher power losses, even if this increase is relatively limited.

V. EXPERIMENTAL VALIDATION

The effectiveness of the proposed control algorithm described in the previous Sections, which can be applied to any m-phase machine, has been experimentally validated through a test bench setup, schematically represented in Fig. 12 and composed of the following elements:

- A 5.5 kW squirrel-cage induction machine, whose parameters and rated values are summarized in Table 4.
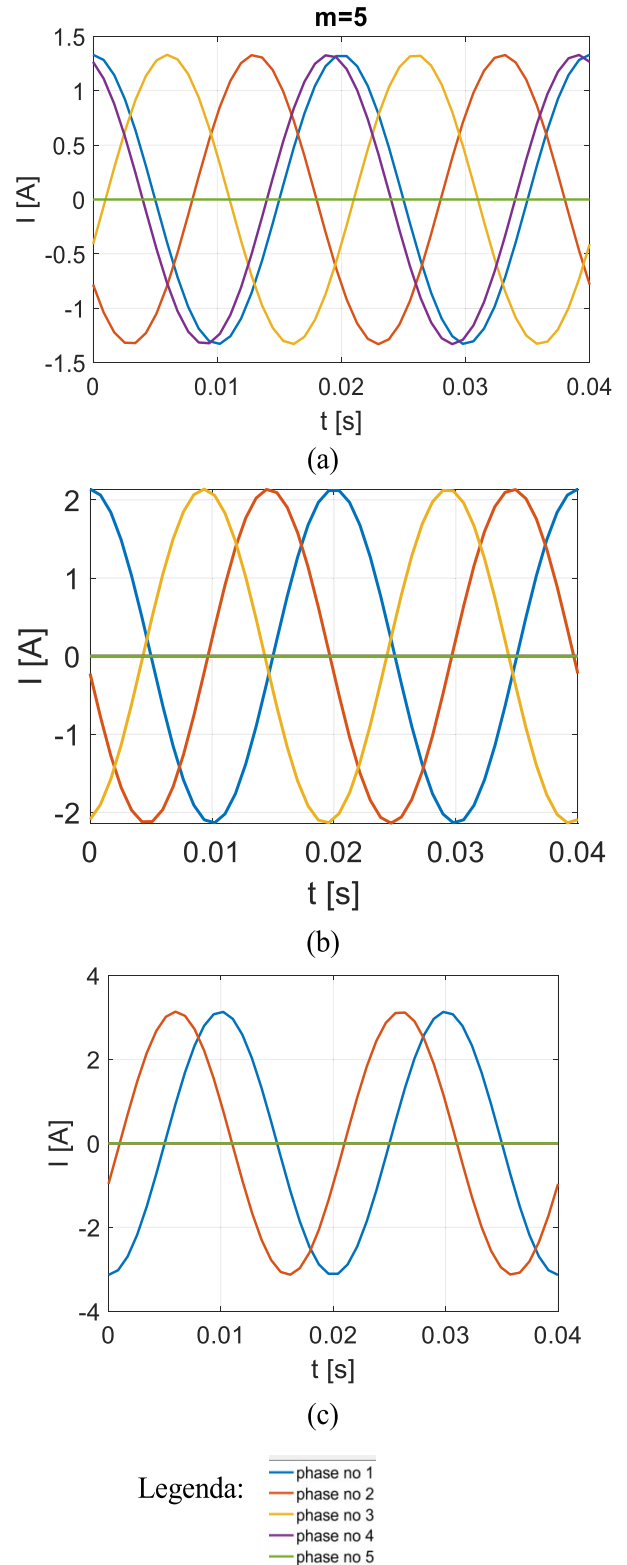
FIGURE 11. Current profiles for: (a) g = 1, (b) g = 2 and (c) g = 3.

- A BF 70/4-22 E-V20 power converter (*Infranor Inc.*), directly connected to the electrical grid, which supplies the electric motor. This converter is composed of a

TABLE 3. FEM results comparison.

	No faults	Fault on phase no 5	Faults on phases no 4 and 5
Overall losses [W]	5.07	9.13	12.12
Average pole flux density [T]	0.63	0.66	0.65
Air-gap magnetic field energy [J]	1.65	1.72	1.71
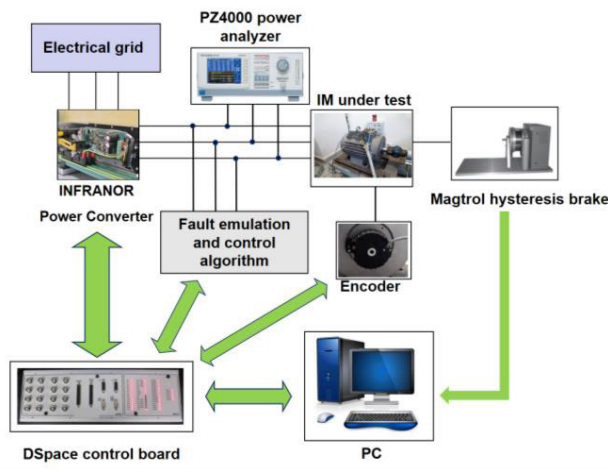
FIGURE 12. Test bench schematics.

rectifying stage and a Voltage Source Inverter to drive the AC machine.

- A PZ4000 power analyzer (*Yokogawa Inc.*) for the real-time detection of the main electrical quantities involved in the system, such as voltages, currents, active power, reactive power and power factor.
- A Fault Emulation System (FES), composed of three relays connected between the power converter and the IM. The state of these electric switches is adequately managed to open one or multiple phases in a specific time instant.
- An EH80 incremental encoder (*Eltra Inc.*) to measure the angular speed of the IM rotor.
- A DSP6001 hysteresis brake (*Magtrol Inc.*), which is connected to the motor and is used to apply a specific mechanical load to the IM taken into account.
- A dSPACE®rapid prototyping board to properly control the components of the power converter and the fault emulation system.
- A PC with the Matlab/Simulink and dSPACE®user interface software to implement and control both the FTA and the FES.

The motor is controlled to operate in different working conditions in terms of both load and speed. The load is set using the hysteresis brake controller, whereas the speed is chosen through the dSPACE user interface by implementing the control strategy shown in Fig. 13. More in detail, the FTA drives the power converter with a reference current
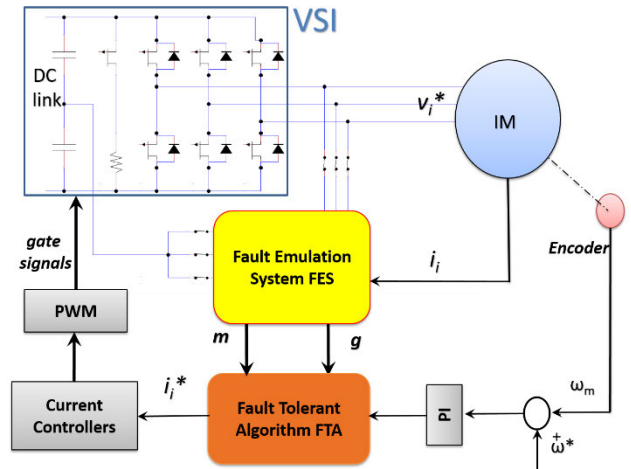
FIGURE 13. Control system schematics.

FIGURE 14. Laboratory setup.

system specifically set in terms of amplitude and phase shifts based on the FTA outputs directly implemented within the control strategy and set from the FES. The output signals from the current controllers will provide the gate signals for the VSI through a traditional PWM technique, which will provide the adequate supply voltages v_i* to the motor. As well as for the FTA control, the emulation of the faults is achieved through the dSPACE board, which controls the state of the previously described relays in the FES connected between the electric motor and the power converter. In the tests hereinafter reported, the open circuit condition has been applied on phase no 3 of the converter; therefore, the motor is supplied with only phases A and B, whereas the current of the faulted phase flows through the DC link capacitors as a return path.

A photograph of the test bench is shown in Fig. 14.

Several tests have been performed with different values of input voltage, switching frequency, load and speed. For instance, Fig. 15 shows the experimental results in terms of phase currents, reference voltages, rotor speed and phase currents trajectories in an α -β stationary frame by applying

TABLE 4. Main rated values of the electric motor under test.

Quantity	Value
Voltage [V]	400
Current [A]	16
Speed [rpm]	2800
Torque [Nm]	18
Power [W]	5500

an open circuit to phase C at 0.1 s driving the system at rated load with a 10 kHz switching frequency and a 50 Hz reference frequency.

It can be noted that, during the fault condition, according to the control strategy of Fig. 13, the current controllers receive the new output motor current signals, which have been varied by the action of the FTA. This aspect leads to a change in the reference voltages, as shown in Fig. 15 (b), in which the two voltage signals of the healthy phases are increased in amplitude and adequately phase-shifted by the control system to satisfy the theoretical procedure described in (9) – (13), whereas the reference voltage on phase 3 equals zero after the fault emulation.

Moreover, the output speed of the motor is not significantly affected by the presence of a fault, as the trend behaves comparably both before and after the fault emulation (Fig. 15 (c)). Regarding the reconfiguration time, it can be observed that the control algorithm can reconfigure the system within a half period, achieving comparable (in certain cases even better) dynamic performance concerning many papers presented in the recent literature [34], [35], [36], [37], [38], [39], [40], [41], [42], [43]. Finally, the space vector diagram for this specific working condition is plotted in Fig. 15 (d).

An important aspect concerns the unbalances in the DC link voltage caused by the presence of the fault condition. As shown in Fig. 15 (c), this unbalance has been compensated by the current controller, capable of generating adequate reference voltages. Moreover, the current distortion occurring in fault conditions causes a change in the magnetic potential, determining an increase in the torque ripple, which can affect the stability of the machine's operation. As reported in many research papers, the fault condition can cause a higher ripple in the current waveforms; in this particular study, the ripple is relatively confined even at full load, confirming the validity of the proposed control algorithm.

Similar results can be appreciated in Fig. 16, which depicts the experimental results concerning the reference voltages and the output speed by applying a 50% rated load and speed emulating a fault at 0.1 s on phase C. As well as for the previous case, the algorithm can re-define the reference voltages to properly drive the motor in the new fault condition, without affecting the speed control. The space vector trajectory for this specific case of study is represented in Fig. 17.
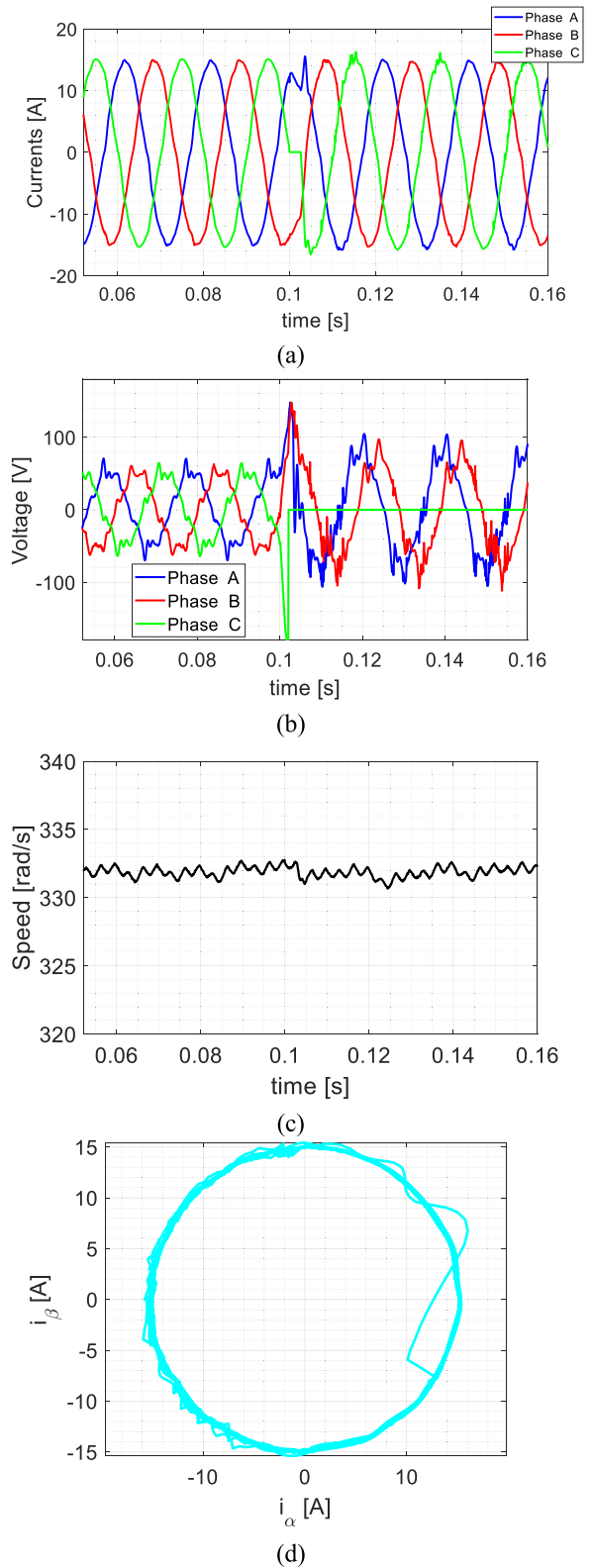
FIGURE 15. Experimental results at rated load and speed with fault emulated at 0.1 s: (a) output currents, (b) reference voltages (c) rotor speed and (d) space vector trajectories.

Finally, Table 5 compares the dynamic performance of the proposed FTA in terms of reconfiguration time with some of
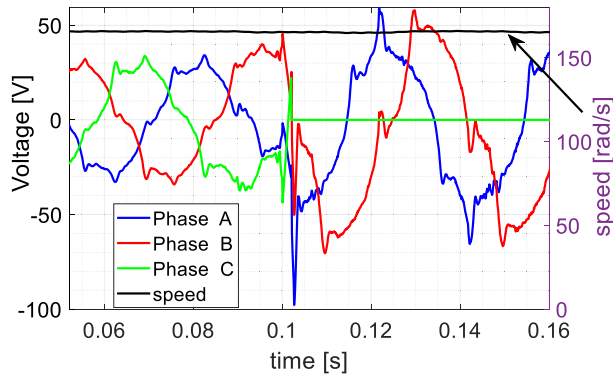
FIGURE 16. Reference voltages and rotor speed results at 50% of both rated load and speed with fault emulated at 0.1 s.
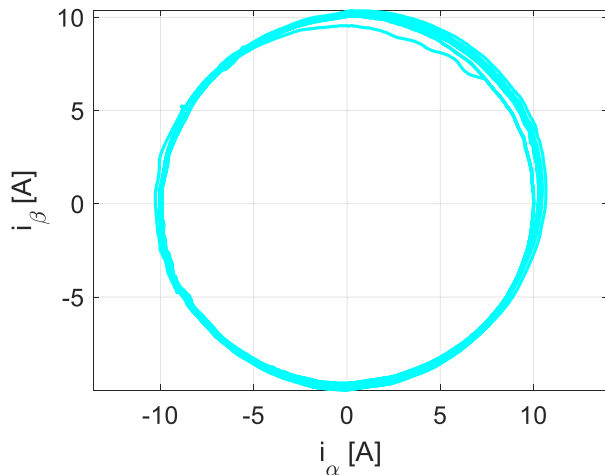
FIGURE 17. Space vector trajectory at 50% of both rated load and speed with fault emulated at 0.1 s.

TABLE 5. Comparison of reconfiguration time.

Fault-tolerant Algorithm	Reconfiguration time [s]
Experimental FTA	0.01
Strategy presented in [35]	0.021
Strategy presented in [36]	0.015
Strategy presented in [37]	0.045
Strategy presented in [38]	0.011
Strategy presented in [39]	0.015
Strategy presented in [40]	0.011

those reported in the recent literature that consider different strategies of fault detection in *m*-phase machines [34], [35], [36], [37], [38], [39], [40], [41], [42], [43] (this comparison has been provided even if, in some cases, the type and the size of the electric machine adopted for the tests can be different).

As shown by the Table, it can be noted that the FTA allows reconfiguring the system within a comparable time with other fault-tolerant algorithms and, in certain cases, the dynamics are also improved.

Therefore, it can be concluded that the FTA provides a robust framework for managing and responding to faults flexibly and dynamically in any application where IPMSM and IM drives are crucial for the correct operation of the whole system.

VI. CONCLUSION

This paper has presented the theoretical analysis, simulation and experimental validation of a simple and flexible fault-tolerant control algorithm for the adequate operation of *m*-phase machines under open circuit faults. After introducing the theory of the magnetic field distribution in polyphase systems, from which the algorithm is conceived, a general formula for the spatial distribution of phase current phasors is then derived and implemented via software. The FEM analysis has demonstrated that the proposed control algorithm does not affect in a significant manner the magnetic performance of the *m*-phase machine, whereas the experimental tests were performed to demonstrate the effectiveness of the proposed procedure with adequate dynamics and reconfiguration time to the strategies reported in the recent literature. It has to be highlighted that the reported control algorithm can be simply and practically applied to any electric machine equipped with a poly-phase winding configuration.

Key findings from the study reveal that the proposed control algorithm is highly adaptable and applicable in electric drives powered by *m*-phase motors, encompassing any configuration of *m*-phase windings, ranging from normal to non-redundant reduced types.

Overall, the study underscores the practicality and efficacy of the proposed procedure in real-world scenarios, providing a valuable contribution to fault-tolerant control strategies for multiphase electric machines.

REFERENCES

[1] E. Levi, R. Bojoi, F. Profumo, H. A. Toliyat, and S. Williamson, "Multiphase induction motor drives—A technology status review," *IET Elect. Power Appl.*, vol. 1, no. 4, pp. 489–516, Jul. 2007.

[2] M. Y. Metwly, A. S. Abdel-Khalik, M. S. Hamad, S. Ahmed, and N. A. Elmalhy, "Multiphase stator winding: New perspectives, advanced topologies, and futuristic applications," *IEEE Access*, vol. 10, pp. 103241–103263, 2022, doi: 10.1109/ACCESS.2022.3209372.

[3] A. M. Silva, F. J. T. E. Ferreira, M. V. Cistelecan, and C. H. Antunes, "Multiobjective design optimization of generalized multilayer multiphase AC winding," *IEEE Trans. Energy Convers.*, vol. 34, no. 4, pp. 2158–2167, Dec. 2019, doi: 10.1109/TEC.2019.2935009.

[4] G. K. Singh, "Multi-phase induction machine drive research—A survey," *Electr. Power Syst. Res.*, vol. 61, no. 2, pp. 139–147, Mar. 2002, doi: 10.1016/s0378-7796(02)00007-x.

[5] E. E. Ward and H. Härer, "Preliminary investigation of an inverter-fed 5-phase induction motor," *Proc. Inst. Electr. Eng.*, vol. 116, pp. 980–984, Jan. 1969.

[6] S. Yang, P. Zheng, Y. Sui, C. Tong, and M. Wang, "Open-circuit fault-tolerant control for pentagon winding connected five-phase current-source inverter based PMSM drives," *IEEE Trans. Ind. Electron.*, vol. 71, no. 3, pp. 2277–2288, Mar. 2023, doi: 10.1109/TIE.2023.3266591.

[7] L. Wu, W. Wang, Z. Lyu, Y. Zhong, and J. Liu, "Coupling effect on unbalanced voltages and power under faulty condition in triple three-phase wind power generators," *IEEE Trans. Ind. Electron.*, vol. 71, no. 2, pp. 1308–1318, Feb. 2023, doi: 10.1109/TIE.2023.3262881.

[8] Y. Chen, C. Liu, S. Liu, and Y. Liu, "Predictive control scheme with adaptive overmodulation for a five-leg VSI driving dual PMSMs," *IEEE Trans. Ind. Electron.*, vol. 71, no. 1, pp. 71–81, Jan. 2023.

[9] M. Adamczyk and T. Orlowska-Kowalska, "Online stator and rotor resistance estimation for current sensor fault-tolerant control of induction motor drives," in *Proc. Int. Conf. Electr. Drives Power Electron. (EDPE)*, High Tatras, Slovakia, Sep. 2023, pp. 1–6.

[10] L. Vancini, M. Mengoni, G. Rizzoli, L. Zarri, and A. Tani, "Fault-tolerant and voltage balancing control for five-phase three-level T-type inverters under open-switch faults," in *Proc. IEEE 14th Int. Symp. Diag. Electr. Mach., Power Electron. Drives (SDEMPED)*, Chania, Greece, Aug. 2023, pp. 465–471, doi: 10.1109/sdemped54949.2023.10271419.

[11] W. Fu, Q. Wu, S. Niu, Y. Chen, and X. Guo, "An enhanced axial-flux magnetic-geared machine with dual-winding design for electric vehicle applications," *CES Trans. Electr. Mach. Syst.*, vol. 7, no. 3, pp. 239–247, Sep. 2023, doi: 10.30941/cestems.2023.00047.

[12] K. Laadjal, F. Bento, J. Serra, and A. J. M. Cardoso, "An integrated strategy for the real-time detection and discrimination of stator inter-turn short-circuits and converter faults in asymmetrical six-phase induction motors," *IEEE Trans. Ind. Appl.*, early access, Jan. 13, 2023, doi: 10.1109/TIA.2023.3321266.

[13] W. Lee and G. Choi, "A comprehensive review of fault-tolerant AC machine drive topologies: Inverter, control, and electric machine," in *Proc. IEEE 13th Int. Symp. Diag. Electr. Mach., Power Electron. Drives (SDEMPED)*, Dallas, TX, USA, vol. 1, Aug. 2021, pp. 269–275.

[14] E. Levi, "Multiphase electric machines for variable-speed applications," *IEEE Trans. Ind. Electron.*, vol. 55, no. 5, pp. 1893–1909, May 2008.

[15] A. M. S. Mendes and A. J. M. Cardoso, "Fault-tolerant operating strategies applied to three-phase induction-motor drives," *IEEE Trans. Ind. Electron.*, vol. 53, no. 6, pp. 1807–1817, Dec. 2006, doi: 10.1109/TIE.2006.885137.

[16] S. Nandi, H. A. Toliyat, and X. Li, "Condition monitoring and fault diagnosis of electrical motors—A review," *IEEE Trans. Energy Convers.*, vol. 20, no. 4, pp. 719–729, Dec. 2005, doi: 10.1109/TEC.2005.847955.

[17] C. Wu, R. Sehab, A. Akrad, and C. Morel, "Fault diagnosis methods and fault tolerant control strategies for the electric vehicle powertrains," *Energies*, vol. 15, no. 13, p. 4840, Jul. 2022, doi: 10.3390/en15134840.

[18] S. Dwari and L. Parsa, "An optimal control technique for multiphase PM machines under open-circuit faults," *IEEE Trans. Ind. Electron.*, vol. 55, no. 5, pp. 1988–1995, May 2008, doi: 10.1109/TIE.2008.920643.

[19] X.-Q. Liu, H.-Y. Zhang, J. Liu, and J. Yang, "Fault detection and diagnosis of permanent-magnet DC motor based on parameter estimation and neural network," *IEEE Trans. Ind. Electron.*, vol. 47, no. 5, pp. 1021–1030, Oct. 2000, doi: 10.1109/41.873210.

[20] G. Demidova, A. Rassõlkin, T. Vaimann, A. Kallaste, J. Zakis, and A. Suzdalenko, "An overview of fuzzy logic approaches for fault diagnosis in energy conversion devices," in *Proc. 28th Int. Workshop Electr. Drives, Improving Rel. Electr. Drives (IWED)*, Moscow, Russia, Jan. 2021, pp. 1–7, doi: 10.1109/IWED52055.2021.9376389.

[21] P. V. Goode and M.-Y. Chow, "Using a neural/fuzzy system to extract heuristic knowledge of incipient faults in induction motors. Part I-methodology," *IEEE Trans. Ind. Electron.*, vol. 42, no. 2, pp. 131–138, Apr. 1995, doi: 10.1109/41.370378.

[22] Z. Ye, B. Wu, and A. R. Sadeghian, "Electrical machine fault detection using adaptive neuro-fuzzy inference," in *Proc. 9th IFSA World Congr., 20th NAFIPS Int. Conf.*, Vancouver, BC, Canada, 2001, pp. 390–394, doi: 10.1109/nafips.2001.944284.

[23] Y. Wu, Z. Zhang, Y. Li, and Q. Sun, "Open-circuit fault diagnosis of six-phase permanent magnet synchronous motor drive system based on empirical mode decomposition energy entropy," *IEEE Access*, vol. 9, pp. 91137–91147, 2021, doi: 10.1109/ACCESS.2021.3090814.

[24] A. Arafat, S. Choi, and J. Baek, "Open-phase fault detection of a five-phase permanent magnet assisted synchronous reluctance motor based on symmetrical components theory," *IEEE Trans. Ind. Electron.*, vol. 64, no. 8, pp. 6465–6474, Aug. 2017, doi: 10.1109/TIE.2017.2682016.

[25] M. Abdel-Akher and K. M. Nor, "Fault analysis of multiphase distribution systems using symmetrical components," *IEEE Trans. Power Del.*, vol. 25, no. 4, pp. 2931–2939, Oct. 2010, doi: 10.1109/TPWRD.2010.2046682.

[26] A. Mohammadpour and L. Parsa, "Global fault-tolerant control technique for multiphase permanent-magnet machines," *IEEE Trans. Ind. Appl.*, vol. 51, no. 1, pp. 178–186, Jan. 2015.

[27] G. G. Rigatos, "A derivative-free Kalman filtering approach to state estimation-based control of nonlinear systems," *IEEE Trans. Ind. Electron.*, vol. 59, no. 10, pp. 3987–3997, Oct. 2012.

[28] S. Stipetic, D. Zarko, and M. Kovacic, "Optimised design of permanent magnet assisted synchronous reluctance motor series using combined analytical–finite element analysis based approach," *IET Electr. Power Appl.*, vol. 10, no. 5, pp. 330–338, May 2016.

[29] N. Bianchi, E. Fornasiero, and S. Bolognani, "Thermal analysis of a five-phase motor under faulty operations," *IEEE Trans. Ind. Appl.*, vol. 49, no. 4, pp. 1531–1538, Jul. 2013.

[30] H. S. Che, M. J. Duran, E. Levi, M. Jones, W.-P. Hew, and N. A. Rahim, "Postfault operation of an asymmetrical six-phase induction machine with single and two isolated neutral points," *IEEE Trans. Power Electron.*, vol. 29, no. 10, pp. 5406–5416, Oct. 2014.

[31] S. Dwari and L. Parsa, "Fault-tolerant control of five-phase permanent-magnet motors with trapezoidal back EMF," *IEEE Trans. Ind. Electron.*, vol. 58, no. 2, pp. 476–485, Feb. 2011.

[32] H. Guzman, M. J. Duran, F. Barrero, B. Bogado, and S. Toral, "Speed control of five-phase induction motors with integrated open-phase fault operation using model-based predictive current control techniques," *IEEE Trans. Ind. Electron.*, vol. 61, no. 9, pp. 4474–4484, Sep. 2014.

[33] J. Pyrhonen, T. Jokinen, and V. Hrabovcova, *Design of Rotating Electrical Machines*. Hoboken, NJ, USA: Wiley, 2008.

[34] G. Sala, P. Girardini, M. Mengoni, L. Zarri, A. Tani, and G. Serra, "Comparison of fault tolerant control techniques for quadruple three-phase induction machines under open-circuit fault," in *Proc. IEEE 11th Int. Symp. Diag. Electr. Mach., Power Electron. Drives (SDEMPED)*, Tinos, Greece, Aug. 2017, pp. 213–219.

[35] G. I. Odnokopylov and A. D. Bragin, "Algorithms of fault tolerant control of induction motor electric drive in phase loss operate mode," in *Proc. Int. Siberian Conf. Control Commun. (SIBCON)*, Omsk, Russia, May 2015, pp. 1–5.

[36] Z. Wei, X. Jiang, S. Yang, X. Zhang, Y. Cai, and S. Wang, "Research on fault-tolerant control strategy of fault-tolerant permanent magnet motor based on cascaded model prediction algorithm," in *Proc. 25th Int. Conf. Electr. Mach. Syst. (ICEMS)*, Chiang Mai, Thailand, Nov. 2022, pp. 1–6.

[37] Z. Peng, Z. Zheng, Y. Li, and Z. Liu, "Sensorless fault-tolerant control of multiphase induction machine using virtual winding and adaptive observer," in *Proc. IEEE Transp. Electrific. Conf. Expo, Asia–Pacific (ITEC Asia–Pacific)*, Harbin, China, Aug. 2017, pp. 1–7.

[38] K. Yu, Y. Fan, J. Chen, and Y. Wang, "Fault-tolerant sensorless control of position sensor failure for permanent magnet Vernier machine," in *Proc. 23rd Int. Conf. Electr. Mach. Syst. (ICEMS)*, Hamamatsu, Japan, Nov. 2020, pp. 1251–1256.

[39] W. Gu, M. Lin, W. Zhang, and C. He, "Fault tolerant control of axial field flux-switching fault tolerant machine under single-phase faults," in *Proc. 20th Int. Conf. Electr. Mach. Syst. (ICEMS)*, Sydney, NSW, Australia, Aug. 2017, pp. 1–6.

[40] G. R. Catuogno, G. O. Garcia, and R. Leidhold, "Fault tolerant control in six-phase PMSM under four open-circuits fault conditions," in *Proc. 42nd Annu. Conf. IEEE Ind. Electron. Soc.*, Florence, Italy, Oct. 2016, pp. 5754–5759.

[41] J. Dusek, P. Arumugam, C. Brunson, E. K. Amankwah, T. Hamiti, and C. Gerada, "Impact of slot/pole combination on inter-turn short-circuit current in fault-tolerant permanent magnet machines," *IEEE Trans. Magn.*, vol. 52, no. 4, pp. 1–9, Apr. 2016.

[42] A. Mohammadpour, S. Mishra, and L. Parsa, "Fault-tolerant operation of multiphase permanent-magnet machines using iterative learning control," *IEEE J. Emerg. Sel. Topics Power Electron.*, vol. 2, no. 2, pp. 201–211, Jun. 2014.

[43] G. Catuogno, L. P. Di Noia, A. Del Pizzo, G. Garcia, and R. Leidhold, "Simple and robust fault tolerant control for open-circuit in high speed PM machines," in *Proc. Int. Symp. Power Electron., Electr. Drives, Autom. Motion (SPEEDAM)*, Amalfi, Italy, Jun. 2018, pp. 950–955.

ANTONINO OSCAR DI TOMMASO was born in Tübingen, Germany, in June 1972. He received the master's and Ph.D. degrees in electrical engineering from the University of Palermo, Italy, in 1999 and 2004, respectively. He was a Postdoctoral Fellow in electrical machines and drives with the Department of Electrical Engineering, University of Palermo, from 2004 to 2006, where he is currently an Associate Professor in electrical machines with the Department of Engineering. His research interests include electrical machines, drives, diagnostics on power converters, and the diagnostics and design of electrical rotating machines.

MASSIMO CARUSO received the M.S. and Ph.D. degrees in electrical engineering from the University of Palermo, Italy, in 2008 and 2012, respectively. In 2011, he joined the MEMS Sensors and Actuators Laboratory Group, University of Maryland, College Park, MD, USA, collaborating for the development of electric micromotors and drives for in vivo bacteria biofilm detection and treatment. In 2014, he joined the Sustainable Development and Energy Saving Laboratory, University of Palermo, focusing his research activities on the design, simulation, and experimental development of electrical machines and drives for industrial and sustainable energy applications, where he is currently a Researcher with the Department of Engineering.

ROSARIO MICELI (Member, IEEE) received the B.S. degree in electrical engineering and the Ph.D. degree from the University of Palermo, Palermo, Italy, in 1982 and 1987, respectively. He is currently a Full Professor in electrical machines with the Polytechnic School, University of Palermo. He is also a Personnel in Charge of the Sustainable Development and Energy Savings Laboratory of the Palermo Athenaeum. His main research interests include the mathematical models of electrical machines, drive system control, and diagnostics, renewable energies, and energy management. He is a Reviewer of IEEE TRANSACTIONS ON INDUSTRIAL ELECTRONICS and IEEE TRANSACTIONS ON INDUSTRY APPLICATIONS.

• • •